Editors' Suggestion

# Gradient Flow for Parton Distribution Functions: First Application to the Pion

Anthony Francis,[1] Patrick Fritzsch,[2] Robert V. Harlander,[3] Rohith Karur,[4,5] Jangho Kim,[6] Jonas T. Kohnen,[3] Giovanni Pederiva,[7,8] Dimitra A. Pefkou,[4,5,*] Antonio Rago,[9] Andrea Shindler,[3,5,4,†] André Walker-Loud,[5,4] and Savvas Zafeiropoulos[10]

[1]*Institute of Physics, National Yang Ming Chiao Tung University, 30010 Hsinchu, Taiwan*
[2]*School of Mathematics, Trinity College, College Green, Dublin, Ireland*
[3]*Institute for Theoretical Particle Physics and Cosmology, TTK, RWTH Aachen University, Sommerfeldstraße 16, Aachen 52074, Germany*
[4]*Department of Physics, University of California, Berkeley, California 94720, USA*
[5]*Nuclear Science Division, Lawrence Berkeley National Laboratory, Berkeley, California 94720, USA*
[6]*Lattice Gauge Theory Research Center, Department of Physics and Astronomy, Seoul National University, Seoul 08826, Korea*
[7]*Jülich Supercomputing Center, Forschungszentrum Jülich, Wilhelm-Johnen-Straße, 54245 Jülich, Germany*
[8]*Center for Advanced Simulation and Analytics (CASA), Forschungszentrum Jülich, Wilhelm-Johnen-Straße, 54245 Jülich, Germany*
[9]*ħQTC & IMADA, University of Southern Denmark, Campusvej 55, 5230 Odense M, Denmark*
[10]*Aix Marseille Univ, Université de Toulon, CNRS, CPT, Marseille, France*

(Received 13 November 2025; revised 2 March 2026; accepted 20 March 2026; published 29 April 2026)

Parton distribution functions (PDFs) are central to precision QCD phenomenology. Their Mellin moments can be computed on the lattice, but direct determinations using local operators, besides $\langle x \rangle$, face severe challenges from reduced hypercubic symmetry, limiting results to the lowest moments. A recently proposed method resolves these issues using gradient flow. We demonstrate the efficacy of this method by computing ratios of flavor nonsinglet pion PDF moments up to $\langle x^5 \rangle$ on four lattice spacings at $m_\pi \simeq 411$ MeV. The moments and reconstructed PDF agree quantitatively with recent phenomenological extractions.

DOI: 10.1103/z3wr-zk8n

*Introduction*—Parton distribution functions (PDFs) have a long history among hadron structure observables, dating back to the discovery of scaling in deep-inelastic scattering at SLAC in the late 1960s. Today, proton PDFs represent one of the dominant sources of uncertainty at several collider experiments [1], underscoring the urgency of improved theoretical input. Moreover, the PDFs of the pion remain much less constrained by experimental data [2–18], since pions cannot be used as fixed targets. Their large-$x$ behavior, often parametrized as $(1-x)^\beta$, has been the subject of long-standing debate and is a strong motivation for upcoming measurements at Jefferson Lab [19] and the Electron-Ion Collider [20,21]. Model calculations typically predict values in the range $\beta = 1$–$2$ [22–46].

The only systematically improvable first-principles approach to calculate hadron structure functions is lattice QCD. In Euclidean space, where lattice QCD is formulated, the nonlocal operators defining PDFs collapse to a point, making their direct computation impossible. A natural approach is to consider Mellin moments,

$$\langle x^{n-1} \rangle_q^h(\mu) = \int_0^1 dx x^{n-1} [q^h(x,\mu) + (-1)^n \bar{q}^h(x,\mu)], \quad (1)$$

with $q^h(x,\mu)$ being a PDF of a hadron $h$ at renormalization scale $\mu$. They can be obtained from matrix elements of local twist-2 operators,

$$\hat{O}^{rs}_{\{\mu_1 \cdots \mu_n\}}(x) = O^{rs}_{\{\mu_1 \cdots \mu_n\}}(x) - \text{traces}, \quad (2)$$

where

$$O^{rs}_{\{\mu_1 \cdots \mu_n\}}(x) = \bar{\psi}^r(x) \gamma_{\{\mu_1} \overleftrightarrow{D}_{\mu_2} \ldots \overleftrightarrow{D}_{\mu_n\}} \psi^s(x), \quad (3)$$

with $\psi^r$ being a quark field of flavor $r$, $\bar{\psi}^s$ an antiquark field of flavor $s$, $\overleftrightarrow{D}_\mu = \frac{1}{2}(\vec{D}_\mu - \overleftarrow{D}_\mu)$ the forward-backward covariant derivative, and $\{\cdots\}$ denoting normalized symmetrization over Lorentz indices.

*Contact author: dpefkou@berkeley.edu
†Contact author: shindler@physik.rwth-aachen.de

*Published by the American Physical Society under the terms of the Creative Commons Attribution 4.0 International license. Further distribution of this work must maintain attribution to the author(s) and the published article's title, journal citation, and DOI. Funded by SCOAP³.*

In the flavor nonsinglet case, there is no mixing with gluonic twist-2 operators, and the moments are obtained from reduced matrix elements of the trace-subtracted operator of Eq. (2) between the hadronic states of interest.

The computation of Mellin moments from local operators has been an active area of lattice QCD research for several decades starting in the 1980s [47–49]. As these early studies already pointed out, additional challenges arise because the O(4) symmetry of the continuum is reduced to the hypercubic symmetry H(4) on the Euclidean lattice.

Accessing the $x$ dependence of PDFs with lattice QCD has seen significant progress in recent decades, with numerous new approaches proposed, including methods to compute Mellin moments from derivatives of Ioffe time distributions [50–69].

In this Letter, we investigate a recently proposed method [70] that employs the gradient flow as an intermediate regulator to compute Mellin moments, and their ratios, of arbitrary order in lattice QCD.

We present the first numerical demonstration of this approach for the flavor nonsinglet pion PDF, thus establishing its practical applicability and effectiveness in lattice calculations. The primary aim of this Letter is to demonstrate a controlled numerical implementation of the method, with particular emphasis on flow-time stability and continuum extrapolations for higher Mellin moments, rather than to provide a complete phenomenological validation. With a modest computational cost, we achieve competitive uncertainties for the lowest moments, extend the direct computation of Mellin moments from local operators up to $n = 6$, and show that a simple PDF reconstruction from these ratios yields results consistent with phenomenological extractions. Our Letter highlights the potential of this approach to extend lattice determinations of PDFs beyond the current state of the art. In the future, these moments can also be incorporated directly into global PDF fits alongside experimental and/or lattice QCD data (see, e.g., Ref. [71]).

*Flowed moments*—The reduction of O(4) to H(4) symmetry on the Euclidean lattice manifests itself in the form of power-divergent operator mixing in calculations of PDF moments. To address this problem, Ref. [70] proposed to use the gradient flow (GF) for the gauge [72–74] and fermion [75] fields. The flow time $t$ acts as an intermediate regulator of ultraviolet divergences: flowed operator matrix elements are finite in the continuum limit if the operator is purely gluonic [73], and they renormalize multiplicatively if fermion fields are present. In the latter case, the renormalization is particularly simple, depending only on the fermion content of the operator [75]. Once the fermion fields are renormalized, one can safely take the continuum limit $a \to 0$ of matrix elements of the flowed operator $\mathcal{O}^{rs}_{\{\mu_1\cdots\mu_n\}}(t,x)$, defined as in Eq. (3) with flowed fields.

In the continuum, these flowed matrix elements can then be related to their physical $t = 0$ counterparts through the short flow-time expansion (SFTX) [76,77] and the corresponding matching coefficients. The matching is simplified and purely multiplicative, making use of the restored $O(4)$ symmetry and its irreducible representations (irreps), by computing matrix elements of flowed traceless twist-2 operators with symmetrization over Lorentz indices, $\hat{\mathcal{O}}^{rs}_{\{\mu_1\cdots\mu_n\}}(t,x)$, defined as in Eq. (2) with flowed fields.

Multiplicative renormalization of the flowed fermion fields can be avoided by considering ratios of matrix elements with identical fermion content. In this way, ratios of PDF moments—e.g., in the $\overline{\text{MS}}$ scheme—can be obtained as

$$\frac{\langle x^{n-1}\rangle^{\overline{\text{MS}}}(\mu)}{\langle x^{m-1}\rangle^{\overline{\text{MS}}}(\mu)} = \frac{\zeta_m(t,\mu)}{\zeta_n(t,\mu)}\frac{\langle x^{n-1}\rangle(t)}{\langle x^{m-1}\rangle(t)} + O(t), \tag{4}$$

where the matching coefficients $\zeta_n(t,\mu)$ were calculated at next-to-leading order (NLO) in Refs. [70,78] and the $O(t)$ terms denote contributions from higher-dimensional operators in the SFTX. The flow-time window for the $t \to 0$ extrapolation is selected using numerical diagnostics, requiring mild linear flow-time dependence after matching and stability under variations of the fit range and lattice spacing. The ratio of flowed moments is directly related to the ratio of reduced matrix elements of the flowed operator, analogous to the $t = 0$ case. It is free from ultraviolet divergences and can be obtained in the continuum limit by keeping the flow time $t$ fixed in physical units. A discussion of the continuum limit and cutoff effects is deferred to Appendix B in the End Matter.

In this Letter, we perform the matching at NNLO up to $n = 6$. The coefficients $\zeta_n(t,\mu)$ of Eq. (4) are determined perturbatively using the method of projectors [79,80], first applied in the context of the gradient flow in Ref. [81]. It leads to scalar two-loop momentum integrals which only depend on the flow time $t$ and the space-time parameter $D = 4 - 2\epsilon$; they can be solved analytically using standard tools (see, e.g., Ref. [82]). Requiring finite $\overline{\text{MS}}$ renormalized matching coefficients confirms the well-known two-loop anomalous dimensions of the twist-2 operators [83,84]. At NLO, we find agreement with the matching coefficients of Refs. [70,76,85]. At NNLO, the results have been known only for the first two moments ($n = 1, 2$) [81,86]; they also agree with our findings. As another check, we verified that our final results for the renormalized matching coefficients are independent of the QCD gauge parameter. The analytical results for the matching coefficients, as well as more details of their calculation, will be deferred to a forthcoming publication.

The strategy can thus be summarized as follows: (*i*) determine the ratios of flowed moments that appear on the rhs of Eq. (4) from lattice QCD using the standard techniques described below, (*ii*) take the continuum limit at fixed flow time $t$, (*iii*) match to the $\overline{\text{MS}}$ scheme at scale $\mu$

TABLE I. Details of the SWF lattice ensembles used in this Letter, which were generated by the OpenLat initiative [88–91], including the total number of gauge configurations, $N_{cfg}$, and the specific source-sink separations, $\tau_s/a$, on which the three-point functions were measured.

| Label | $a$ (fm) | $t_0/a^2$ | $\beta$ | $\kappa_{ud}=\kappa_s$ | $T/a\times(L/a)^3$ | $N_{cfg}$ | $\tau_s/a$ |
|---|---|---|---|---|---|---|---|
| a12m412_mL6.0 | 0.12 | 1.4868(04) | 3.685 | 0.1394305 | $96\times 24^3$ | 838 | 35, 40 |
| a094m412_mL6.2 | 0.094 | 2.4400(01) | 3.8 | 0.138963 | $96\times 32^3$ | 700 | 35, 40 |
| a077m412_mL7.7 | 0.077 | 3.6239(12) | 3.9 | 0.138603 | $96\times 48^3$ | 400 | 40, 42 |
| a064m412_mL6.4 | 0.064 | 5.2471(26) | 4.0 | 0.138272 | $96\times 48^3$ | 500 | 40, 42 |

using the coefficients $\zeta_n(t,\mu)$ in Eq. (4), and (*iv*) analyze the resulting ratio of PDF moments as a function of $t$; if a residual $t$-dependence remains, extrapolate to $t\to 0$ to obtain the physical result. In this Letter, we present the main results of this procedure, while additional details of each step are given in a companion paper [87].

*Lattice QCD calculation*—The matching described in the previous section is independent of the choice of Lorentz indices of the flowed twist-2 operators. To optimize the signal-to-noise ratio, we compute matrix elements of operators with only temporal Euclidean components, $\hat{\mathcal{O}}^{rs}_n=\hat{\mathcal{O}}^{rs}_{4\ldots 4}$, where $n$ temporal indices are implied, made traceless by subtracting the appropriate spatial or mixed components [70]. For this operator choice, no external three-momentum is required, and the flowed moments are related to matrix elements via

$$\frac{\langle x^{n-1}\rangle(t)}{\langle x^{m-1}\rangle(t)}=\frac{(-1)^{n-m}}{m_h^{n-m}}\frac{\langle h(\mathbf{0})|\hat{\mathcal{O}}^{uu}_n(t)|h(\mathbf{0})\rangle}{\langle h(\mathbf{0})|\hat{\mathcal{O}}^{uu}_m(t)|h(\mathbf{0})\rangle}, \tag{5}$$

where the factor $(-1)^{n-m}$ accounts for the Euclidean metric. To extract the matrix elements of Eq. (5) for the pion, we compute the connected three-point functions

$$C^{uu}_n(t;x_4=\tau_s,y_4=\tau_{\mathcal{O}}) = a^6\sum_{\mathbf{x},\mathbf{y}}\langle P^{du}(\mathbf{x},x_4)\hat{\mathcal{O}}^{uu}_n(t,\mathbf{y},y_4)P^{ud}(0)\rangle_c, \tag{6}$$

projected to zero spatial momentum for all $n$. Here, $P^{ud}(x)=\bar{\psi}^u(x)\gamma_5\psi^d(x)$ denotes an interpolating operator with the quantum numbers of a $\pi^+$ state.

On a hypercubic lattice, the O(4) representation, when restricted to H(4), decomposes into a direct sum of H(4) irreps. This implies that different discretizations of traceless, Lorentz-symmetric operators are possible. Although all such choices share the same continuum limit, this freedom could in principle be exploited to reduce discretization effects. Here, we restrict to the standard O(4) irrep for all $n$, leaving a numerical study of alternative discretizations to future work.

We compute three-point functions for $n\in\{2,3,4,5,6\}$ using four stabilized Wilson fermion (SWF) ensembles generated by the OpenLat initiative [88–91]. These ensembles span four lattice spacings, $a\simeq[0.12,0.094,0.077,0.064]$ fm, with the lattice scale set from $t_0/a^2$ [73] and converted to physical units using $\sqrt{t_0}=0.14474(57)$ fm [92–96]. They are generated with $N_f=3$ degenerate dynamical quarks, tuned such that the pion mass is $m_\pi\simeq 411$ MeV. The number of independent configurations and other run parameters for each ensemble are listed in Table I. Further technical details of the lattice QCD calculation are given in Appendix A in the End Matter.

We are interested in determining ratios of matrix elements for the ground state, [97] $A_n(t)/A_2(t)$, where $A_n(t)\equiv\langle\pi(\mathbf{0})|\hat{\mathcal{O}}^{uu}_n(t)|\pi(\mathbf{0})\rangle$. To isolate the ground state, we assume the limit $\tau_s\gg\tau_{\mathcal{O}}\gg 0$, which ensures ground-state dominance. In this regime, for each flow time $t/a^2$, the ratio of three-point functions becomes

$$\frac{C^{uu}_n(t;\tau_s,\tau_{\mathcal{O}})}{C^{uu}_2(t;\tau_s,\tau_{\mathcal{O}})}\simeq\frac{A_n(t)}{A_2(t)}+\cdots, \tag{7}$$

where the ellipsis denotes excited-state contributions. We then look for plateau-like behavior as a function of the operator insertion time $\tau_{\mathcal{O}}$ for each source-sink separation $\tau_s$. As an effective estimator of $A_n(t)/A_2(t)$, we use an average over all $(\tau_s,\tau_{\mathcal{O}})$ values of the ratios with $\tau_s/2-2\le\tau_{\mathcal{O}}\le\tau_s/2+2$, with an additional systematic error equal to the half-difference between the maximum and minimum central value of the averaged-together ratios. Further details on this choice and on excited-state contamination are given in the End Matter and in the companion publication [87].

*Moment results*—To obtain the flowed moment ratios, we multiply our final results $A_n(t)/A_2(t)$ by the appropriate factors involving the pion mass in lattice units, as defined in Eq. (5). The resulting ratios are extrapolated to the continuum limit, assuming cutoff effects of $O(a^2)$. The outcome is shown in Fig. 4 in the End Matter, where results for individual ensembles at each lattice spacing are displayed together with the extrapolated $a\to 0$ values (black circles). Further details on the continuum extrapolation and the choice of the minimal value $(t/t_0)_{\min}$ are provided in the End Matter.

Finally, we multiply the continuum-extrapolated values of each ratio by the matching factors to the $\overline{\text{MS}}$ scheme at the scale $\mu=2$ GeV, and we examine the results for

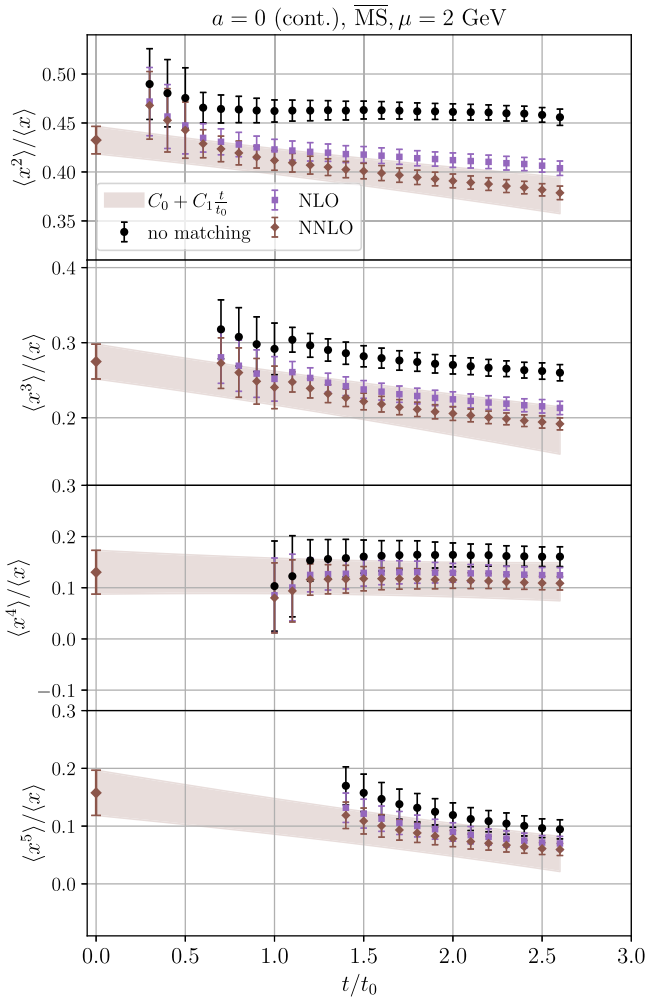



FIG. 1. Continuum-extrapolated ratios of Mellin moments $\langle x^{n-1}\rangle/\langle x\rangle$ for $n = 3$, 4, 5, 6 as functions of the flow time $t/t_0$. Black points show the continuum limit without matching, while purple and brown points correspond to NLO and NNLO matching, respectively, in the $\overline{\text{MS}}$ scheme at $\mu = 2$ GeV. The shaded bands indicate the outcome of the fit procedure, where multiple fits of the form $C_0 + C_1 t/t_0$ over different ranges of the NNLO matched ratios are combined with equal weights to estimate the physical $t \to 0$ limit.

residual flow-time dependence. This is shown in Fig. 1, where we display the continuum results before matching (black circles), and after matching at NLO (purple squares) and NNLO (brown diamonds). The NNLO-matched results are then extrapolated to $t = 0$, using a linear fit in $t/t_0$. The flow-time window for the $t/t_0 \to 0$ extrapolation is selected using numerical diagnostics, requiring mild linear flow-time dependence after matching and stability under variations of the fit range and lattice spacing. The fit ranges are taken as all possible intervals within $[(t/t_0)_{\text{min}}, 2.6]$, where $(t/t_0)_{\text{min}}$ for each $n$ are defined in Fig. 4, with a minimum fit range in $t/t_0$ of at least 0.8. Each fit with $p$-value $> 0.1$ is weighted equally as a conservative choice, and the shaded bands represent the combined outcome of this procedure.

TABLE II. *Top*: Final results for $\langle x^{n-1}\rangle/\langle x\rangle$ in the $\overline{\text{MS}}$ scheme at $\mu = 2$ GeV. *Bottom:* Parameters of the PDF reconstruction fits (see Fig. 3), performed using the ansatz of Eq. (8), either including ($n_{\text{max}} = 6$) or excluding ($n_{\text{max}} = 5$) the highest-order moment ratio.

| $n$ | 3 | 4 | 5 | 6 |
|---|---|---|---|---|
| $\langle x^{n-1}\rangle/\langle x\rangle$ | 0.433(14) | 0.275(23) | 0.130(43) | 0.158(39) |
| | Fit with $n_{\text{max}} = 6$ | | Fit with $n_{\text{max}} = 5$ | |
| $\alpha$ | −0.48(10) | | −0.47(11) | |
| $\beta$ | 0.93(16) | | 0.97(17) | |

The results of this analysis constitute our final estimates for $\langle x^{n-1}\rangle/\langle x\rangle$ in the $\overline{\text{MS}}$ scheme at $\mu = 2$ GeV, and are listed in Table II.

In Fig. 2, we compare our results with recent phenomenological determinations [9,14,18,98]. Perfect agreement is not expected, since our calculation is performed at a heavier-than-physical pion mass of $m_\pi \simeq 411$ MeV. Guidance on the pion-mass dependence can be drawn from previous lattice QCD studies [99–104], which show inconsistent $m_\pi$ trends for the moments and ratios, and no clearly preferred chiral behavior. A systematic investigation of the chiral dependence is deferred to future work.

A comparison with other direct lattice QCD calculations is presented in Table III. References [105,106] employ states boosted in multiple directions to avoid power-divergent mixing with lower-dimensional operators, which

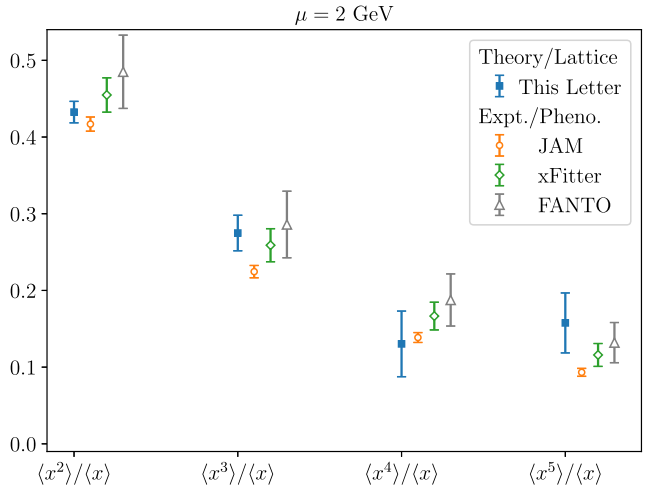



FIG. 2. Comparison of our continuum-extrapolated results from Table II for the pion PDF moment ratios $\langle x^{n-1}\rangle/\langle x\rangle$ at $\mu = 2$ GeV (blue squares), obtained at a pion mass of $m_\pi \simeq 411$ MeV, with phenomenological extractions of the valence sector from JAM (orange circles) [14], xFitter (green diamonds) [9], and FANTO (gray triangles) [18], all obtained from global fits to experimental data.

TABLE III. Comparison with twist-2 operator determinations from ETMC [105,106], derivatives of Ioffe time distributions from HadStruc [63] and BNL [67]. For the results of Ref. [63], covariances between the moments are not available and have been neglected in the shown ratios.

| | $N_f$ | $m_\pi$ [MeV] | $a$ [fm] | $\langle x^2\rangle/\langle x\rangle$ | $\langle x^3\rangle/\langle x\rangle$ | $\langle x^3\rangle/\langle x^2\rangle$ | $\langle x^4\rangle/\langle x\rangle$ | $\langle x^4\rangle/\langle x^2\rangle$ |
|---|---|---|---|---|---|---|---|---|
| This Letter | 3 | 411 | Cont. | 0.433(14) | 0.275(23) | 0.636(50) | 0.130(43) | 0.301(98) |
| ETMC [105] | $2+1+1$ | 260 | 0.093 | 0.30(11) | | | | |
| ETMC [106] | $2+1+1$ | 260 | 0.093 | | 0.092(71) | 0.22(17) | | |
| HadStruc [63] | $2+1$ | 415 | 0.127 | 0.370(47) | 0.224(16) | | 0.059(47) | |
| BNL [67] | $2+1$ | 140 | Cont.[a] | | | | | 0.351(34) |

[a]The continuum limit is estimated using calculations at $a = 0.076$ fm with, $m_\pi = 140$ MeV, and at $a = 0.04$ and 0.06 fm with $m_\pi = 300$ MeV.

leads to signals that are significantly noisier than ours. References [63,67] instead use Ioffe time distributions to extract PDF moments. The discrepancies between different lattice QCD computations are not worrisome, because calculations are done with different pion masses, different numbers of dynamical flavors, and in some cases with systematics not completely under control.

While this Letter is a proof-of-principle calculation, we nevertheless identify potential sources of systematic effects to be investigated further once the statistical precision is increased and more data becomes available. In addition to the conservatively treated excited-state contamination, in our calculation we perform a robust continuum extrapolation at an unphysical pion mass. Cutoff effects grow, as expected, at small flow times; however, in the region where they are under control, we observe that the relative difference between NLO and NNLO corrections is about 5%, and that the $t \to 0$ extrapolation is stable with respect to variations of the fit range in flow time. This is reassuring for future calculations with higher precision. Extending the region where a controlled continuum limit can be taken toward smaller flow times, thereby enabling more stringent tests of the short-flow-time expansion, is an important direction for future work.

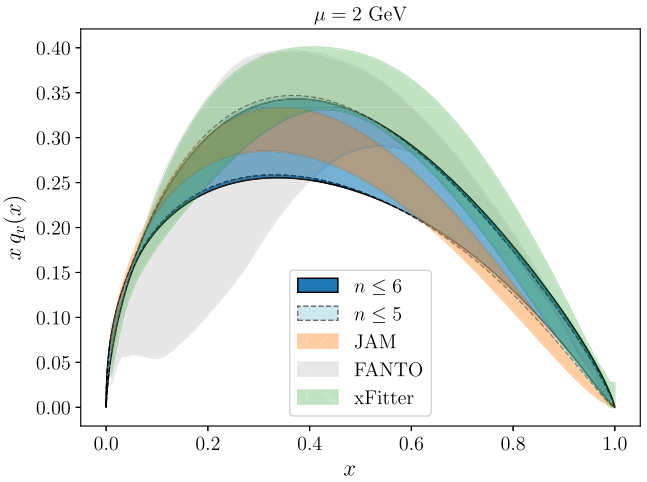



FIG. 3. Reconstructed pion valence PDF $q_v(x) \propto x^\alpha(1-x)^\beta$ obtained by fitting the parameters $\alpha$ and $\beta$ to the ratios of moments computed in this Letter. The blue band uses all available moments up to $n = 6$, while the light-blue band excludes the highest ratio $\langle x^5\rangle/\langle x\rangle$. For comparison, we also show phenomenological extractions from JAM, xFitter, and FANTO [9,14,18], respectively.

*PDF reconstruction*—Given our results for the ratios of moments in Table II, we attempt a reconstruction of the PDF using the simple ansatz [6,107]

$$q_v(x) \propto x^\alpha(1-x)^\beta \tag{8}$$

and fit our data to the analytic dependence of the moments on $\alpha$ and $\beta$. As expected, the fitting procedure is nontrivial: while Gaussian priors help stabilize the fit, the results remain highly sensitive to the prior width of $\alpha$. We also find that excluding the highest-order moment ($n = 6$) has little impact on the extracted values of $\alpha$ and $\beta$, shown in Table II, indicating that higher moments affect these parameters only weakly unless determined with higher precision.

The resulting PDF, shown in Fig. 3, is in reasonable agreement with phenomenological extractions [9,14,18], but, for the reasons discussed above, should be regarded as illustrative rather than a robust reconstruction. Despite these limitations, it is worth noting that the preferred values for $\beta$ are $\sim$1, in support of some of the recent determinations [9,14,71].

*Summary and conclusion*—We have presented the first direct lattice QCD extraction of the flavor nonsinglet pion PDF moment ratios $\langle x^{n-1}\rangle/\langle x\rangle$ for $n \in [3, 6]$, using a novel method [70] that employs the gradient flow as an intermediate regulator. Our results for the moment ratios show full agreement with phenomenological extractions. The precision achieved with a modest statistical sample is already comparable to phenomenology, opening the possibility of incorporating lattice QCD results from this method into global PDF fits [71], either directly in the form of ratios as presented here or as individual moments. In the latter case, determination of the normalization $\langle x\rangle$ is required; this can be obtained with standard lattice QCD techniques and renormalized in the $\overline{\text{MS}}$ scheme either via the regularization-independent momentum-subtraction

(RI-MOM) procedure [108,109] or by renormalizing the flowed fermion fields.

This Letter demonstrates the viability of the method and provides meaningful results; a more detailed study of systematic effects will become necessary once higher statistical precision is achieved. Future investigations will include (*i*) the impact of excited-state contamination, (*ii*) a better understanding of cutoff effects and their possible reduction by exploiting different discretizations of the twist-2 operators based on the subduced hypercubic irreps, (*iii*) a dedicated study of the pion-mass dependence toward the physical point, and (*iv*) the impact of higher-order corrections in the perturbative matching. The PDF reconstruction from our results could also benefit from Bayesian approaches, such as Gaussian processes [110,111], which have the potential to stabilize the fits and provide less model-dependent reconstructions compared to the current parametric ansatz.

In addition to solving a long-standing challenge in the field, this method is complementary to other promising approaches [50–59], and combining results from both should substantially enhance the impact of lattice QCD in this area.

Finally, this Letter opens the way for applying this method to other quantities of interest, including the proton PDFs, the flavor-singlet and gluon PDFs, and off-forward structure functions such as the generalized parton distributions [112,113].

*Acknowledgments*—We thank Wally Melnitchouk for useful discussions on the reconstruction of PDFs from moments, and Martin Hoferichter for discussions on the chiral dependence of moments of PDFs. We thank the authors of Refs. [14,67] for providing their data. All phenomenological results in the comparison plots were obtained using the LHAPDF6 library [114]. Numerical calculations for this work were performed using resources from the National Energy Research Scientific Computing Center (NERSC), a Department of Energy Office of Science User Facility, under NERSC Awards No. NP-ERCAP0024080 and No. NP-ERCAP0027662. The authors gratefully acknowledge the Gauss Centre for Supercomputing e.V. [115] for funding the projects "Hadron structure with stabilized Wilson fermions" and "Hadron Structure and Fundamental Symmetries in Lattice QCD" by providing computing time through the John von Neumann Institute for Computing (NIC) on the GCS Supercomputer JUWELS [116] at the Jülich Supercomputing Centre (JSC). We also acknowledge the EuroHPC Joint Undertaking for awarding this project access to the EuroHPC supercomputer LEONARDO, hosted by CINECA (Italy) and LUMI at CSC (Finland). The authors acknowledge support, as well as computing and storage resources by GENCI on Adastra and Occigen (CINES), Jean-Zay (IDRIS), and Irène-Joliot-Curie (TGCC) under Projects No. (2020-2024)-A0080511504, No. (2020-2024)-A0080502271, and No. 2025-A0180516207. A. F. acknowledges support by the National Science and Technology Council of Taiwan under Grants No. 113-2112-M-A49-018-MY3 and No. 111-2112-M-A49-018-MY2. The work of R. K. is supported in part by the NSF Graduate Research Fellowship Program under Grant No. DGE-2146752 and by the DOE NNSA LRGF Fellowship under Cooperative Agreement No. DE-NA0003960. This research was supported by the National Research Foundation (NRF) funded by the Korean government (MSIT) (No. RS-2025-02221606). R. V. H. and J. T. K. acknowledge support by the Deutsche Forschungsgemeinschaft (DFG, German Research Foundation) under Grants No. 460791904 and No. 396021762—TRR 257 "Particle Physics Phenomenology after the Higgs Discovery." G. P. acknowledges funding by the Deutsche Forschungsgemeinschaft (DFG, German Research Foundation) Project No. 460248186 (PUNCH4NFDI). D. A. P. is supported from the Office of Nuclear Physics, Department of Energy, under Contract No. DE-SC0004658. A. S. acknowledges funding support from Deutsche Forschungsgemeinschaft (DFG, German Research Foundation) through Grant No. 513989149 and under National Science Foundation Grant No. PHY-2209185. The work of R. K., D. A. P., A. S., and A. W.-L. was supported by the U.S. Department of Energy, Office of Science, Office of Nuclear Physics, under Contract No. DE-AC02-05CH11231. The research of S. Z. is funded, in part, by l'Agence Nationale de la Recherche (ANR), Project No. ANR-23-CE31-0019. We acknowledge support from the DOE Topical Collaboration "Nuclear Theory for New Physics," Award No. DE-SC0023663. This manuscript was finalized at the Aspen Center for Physics, which is supported by National Science Foundation Grant No. PHY-2210452. The OpenQCD [117], Chroma [118], QUDA [119–121], QDP-JIT [122], and LALIBE [123] software libraries were used in this Letter. Data analysis used NumPy [124], SciPy [125], GVAR [126], and LSQFIT [127]. Figures were produced using MATPLOTLIB [128].

*Data availability*—The data that support the findings of this article are not publicly available upon publication because it is not technically feasible and/or the cost of preparing, depositing, and hosting the data would be prohibitive within the terms of this research project. The data are available from the authors upon reasonable request.

[1] S. Amoroso *et al.*, Snowmass 2021 whitepaper: Proton structure at the precision frontier, Acta Phys. Pol. B **53**, 12 (2022).

[2] J. S. Conway *et al.*, Experimental study of muon pairs produced by 252-GeV pions on tungsten, Phys. Rev. D **39**, 92 (1989).

[3] B. Betev *et al.* (NA10 Collaboration), Differential cross-section of high mass muon pairs produced by a

194-GeV/$c\pi^-$ beam on a tungsten target, Z. Phys. C **28**, 9 (1985).
[4] J. F. Owens, $Q^2$ dependent parametrizations of pion parton distribution functions, Phys. Rev. D **30**, 943 (1984).
[5] P. Aurenche, R. Baier, M. Fontannaz, M. Kienzle-Focacci, and M. Werlen, The gluon content of the pion from high-$p_t$ photon production, Phys. Lett. B **233**, 517 (1989).
[6] P. J. Sutton, A. D. Martin, R. G. Roberts, and W. J. Stirling, Parton distributions for the pion extracted from Drell-Yan and prompt photon experiments, Phys. Rev. D **45**, 2349 (1992).
[7] M. Glück, E. Reya, and A. Vogt, Pionic parton distributions, Z. Phys. C **53**, 651 (1992).
[8] K. Wijesooriya, P. E. Reimer, and R. J. Holt, The pion parton distribution function in the valence region, Phys. Rev. C **72**, 065203 (2005).
[9] I. Novikov *et al.*, Parton distribution functions of the charged pion within the xFitter framework, Phys. Rev. D **102**, 014040 (2020).
[10] F. D. Aaron *et al.* (H1 Collaboration), Measurement of leading neutron production in deep-inelastic scattering at HERA, Eur. Phys. J. C **68**, 381 (2010).
[11] S. Chekanov *et al.* (ZEUS Collaboration), Leading neutron production in e + p collisions at HERA, Nucl. Phys. **B637**, 3 (2002).
[12] P. C. Barry, N. Sato, W. Melnitchouk, and C.-R. Ji, First Monte Carlo global QCD analysis of pion parton distributions, Phys. Rev. Lett. **121**, 152001 (2018).
[13] N. Y. Cao, P. C. Barry, N. Sato, and W. Melnitchouk (Jefferson Lab Angular Momentum Collaboration), Towards the three-dimensional parton structure of the pion: Integrating transverse momentum data into global QCD analysis, Phys. Rev. D **103**, 114014 (2021).
[14] P. C. Barry, C.-R. Ji, N. Sato, and W. Melnitchouk (Jefferson Lab Angular Momentum (JAM) Collaboration), Global QCD analysis of pion parton distributions with threshold resummation, Phys. Rev. Lett. **127**, 232001 (2021).
[15] M. Aicher, A. Schäfer, and W. Vogelsang, Soft-gluon resummation and the valence parton distribution function of the pion, Phys. Rev. Lett. **105**, 252003 (2010).
[16] D. Westmark and J. F. Owens, Enhanced threshold resummation formalism for lepton pair production and its effects in the determination of parton distribution functions, Phys. Rev. D **95**, 056024 (2017).
[17] L. Kotz, A. Courtoy, P. Nadolsky, F. Olness, and M. Ponce-Chavez, Analysis of parton distributions in a pion with Bézier parametrizations, Phys. Rev. D **109**, 074027 (2024).
[18] L. Kotz, A. Courtoy, P. Nadolsky, and M. Ponce-Chavez, Fantômas: Epistemic and nuclear uncertainties for the parton distributions of the pion, Phys. Rev. D **112**, L071502 (2025).
[19] R. A. Montgomery, J. R. M. Annand, D. Dutta, C. E. Keppel, P. King, B. Wojtsekhowski, and J. Zhang (TDIS, SBS Collaborations), Proposed measurement of tagged deep inelastic scattering in Hall A of Jefferson lab, AIP Conf. Proc. **1819**, 030004 (2017).
[20] R. Abdul Khalek *et al.*, Science requirements and detector concepts for the electron-ion collider: EIC Yellow Report, Nucl. Phys. **A1026**, 122447 (2022).
[21] J. Arrington *et al.*, Revealing the structure of light pseudoscalar mesons at the electron–ion collider, J. Phys. G **48**, 075106 (2021).
[22] Z. F. Ezawa, Wide-angle scattering in softened field theory, Nuovo Cimento A **23**, 271 (1974).
[23] P. V. Landshoff and J. C. Polkinghorne, Threshold properties of electroproduction and annihilation, Nucl. Phys. **B53**, 473 (1973).
[24] J. F. Gunion, S. J. Brodsky, and R. Blankenbecler, Large angle scattering and the interchange force, Phys. Rev. D **8**, 287 (1973).
[25] G. R. Farrar and D. R. Jackson, The pion form-factor, Phys. Rev. Lett. **43**, 246 (1979).
[26] E. L. Berger and S. J. Brodsky, Quark structure functions of mesons and the Drell-Yan process, Phys. Rev. Lett. **42**, 940 (1979).
[27] T. Shigetani, K. Suzuki, and H. Toki, Pion structure function in the Nambu and Jona-Lasinio model, Phys. Lett. B **308**, 383 (1993).
[28] A. Szczepaniak, C.-R. Ji, and S. R. Cotanch, Generalized relativistic meson wave function, Phys. Rev. D **49**, 3466 (1994).
[29] R. M. Davidson and E. Ruiz Arriola, Structure functions of pseudoscalar mesons in the SU(3) NJL model, Phys. Lett. B **348**, 163 (1995).
[30] M. B. Hecht, C. D. Roberts, and S. M. Schmidt, Valence quark distributions in the pion, Phys. Rev. C **63**, 025213 (2001).
[31] W. Melnitchouk, Quark hadron duality in electron pion scattering, Eur. Phys. J. A **17**, 223 (2003).
[32] S. Noguera and S. Scopetta, Pion transverse momentum dependent parton distributions in the Nambu and Jona-Lasinio model, J. High Energy Phys. 11 (2015) 102.
[33] P. T. P. Hutauruk, I. C. Cloet, and A. W. Thomas, Flavor dependence of the pion and kaon form factors and parton distribution functions, Phys. Rev. C **94**, 035201 (2016).
[34] T. J. Hobbs, Quantifying finite-momentum effects in the quark quasidistribution functions of mesons, Phys. Rev. D **97**, 054028 (2018).
[35] G. F. de Teramond, T. Liu, R. S. Sufian, H. G. Dosch, S. J. Brodsky, and A. Deur (HLFHS Collaboration), Universality of generalized parton distributions in light-front holographic QCD, Phys. Rev. Lett. **120**, 182001 (2018).
[36] K. D. Bednar, I. C. Cloët, and P. C. Tandy, Distinguishing quarks and gluons in pion and kaon parton distribution functions, Phys. Rev. Lett. **124**, 042002 (2020).
[37] J. Lan, C. Mondal, S. Jia, X. Zhao, and J. P. Vary, Parton distribution functions from a light front Hamiltonian and QCD evolution for light mesons, Phys. Rev. Lett. **122**, 172001 (2019).
[38] J. Lan, C. Mondal, S. Jia, X. Zhao, and J. P. Vary, Pion and kaon parton distribution functions from basis light front quantization and QCD evolution, Phys. Rev. D **101**, 034024 (2020).
[39] L. Chang, K. Raya, and X. Wang, Pion parton distribution function in light-front holographic QCD, Chin. Phys. C **44**, 114105 (2020).
[40] Z.-F. Cui, M. Ding, F. Gao, K. Raya, D. Binosi, L. Chang, C. D. Roberts, J. Rodríguez-Quintero, and S. M. Schmidt,

Kaon and pion parton distributions, Eur. Phys. J. C **80**, 1064 (2020).
[41] A. Kock, Y. Liu, and I. Zahed, Pion and kaon parton distributions in the QCD instanton vacuum, Phys. Rev. D **102**, 014039 (2020).
[42] Z. F. Cui, M. Ding, J. M. Morgado, K. Raya, D. Binosi, L. Chang, F. De Soto, C. D. Roberts, J. Rodríguez-Quintero, and S. M. Schmidt, Emergence of pion parton distributions, Phys. Rev. D **105**, L091502 (2022).
[43] L. Albino, I. M. Higuera-Angulo, K. Raya, and A. Bashir, Pseudoscalar mesons: Light front wave functions, GPDs, and PDFs, Phys. Rev. D **106**, 034003 (2022).
[44] M. Ahmady, S. Kaur, C. Mondal, and R. Sandapen, Pion spectroscopy and dynamics using the holographic light-front Schrödinger equation and the 't Hooft equation, Phys. Lett. B **836**, 137628 (2023).
[45] B. Pasquini, S. Rodini, and S. Venturini [MAP (Multi-dimensional Analyses of Partonic distributions) Collaboration], Valence quark, sea, and gluon content of the pion from the parton distribution functions and the electromagnetic form factor, Phys. Rev. D **107**, 114023 (2023).
[46] Y. Lu, Y.-Z. Xu, K. Raya, C. D. Roberts, and J. Rodríguez-Quintero, Pion distribution functions from low-order Mellin moments, Phys. Lett. B **850**, 138534 (2024).
[47] A. S. Kronfeld and D. M. Photiadis, Phenomenology on the lattice: Composite operators in lattice gauge theory, Phys. Rev. D **31**, 2939 (1985).
[48] G. Martinelli and C. T. Sachrajda, Pion structure functions from lattice QCD, Phys. Lett. B **196**, 184 (1987).
[49] G. Martinelli and C. T. Sachrajda, A lattice study of nucleon structure, Nucl. Phys. **B316**, 355 (1989).
[50] U. Aglietti, M. Ciuchini, G. Corbo, E. Franco, G. Martinelli, and L. Silvestrini, Model independent determination of the shape function for inclusive B decays and of the structure functions in DIS, Phys. Lett. B **432**, 411 (1998).
[51] W. Detmold and C. J. D. Lin, Deep-inelastic scattering and the operator product expansion in lattice QCD, Phys. Rev. D **73**, 014501 (2006).
[52] X. Ji, Parton physics on a Euclidean lattice, Phys. Rev. Lett. **110**, 262002 (2013).
[53] C. Monahan and K. Orginos, Locally smeared operator product expansions in scalar field theory, Phys. Rev. D **91**, 074513 (2015).
[54] A. Radyushkin, Nonperturbative evolution of parton quasi-distributions, Phys. Lett. B **767**, 314 (2017).
[55] K. Orginos, A. Radyushkin, J. Karpie, and S. Zafeiropoulos, Lattice QCD exploration of parton pseudo-distribution functions, Phys. Rev. D **96**, 094503 (2017).
[56] A. J. Chambers, R. Horsley, Y. Nakamura, H. Perlt, P. E. L. Rakow, G. Schierholz, A. Schiller, K. Somfleth, R. D. Young, and J. M. Zanotti, Nucleon structure functions from operator product expansion on the lattice, Phys. Rev. Lett. **118**, 242001 (2017).
[57] V. Braun and D. Müller, Exclusive processes in position space and the pion distribution amplitude, Eur. Phys. J. C **55**, 349 (2008).
[58] Y.-Q. Ma and J.-W. Qiu, Extracting parton distribution functions from lattice QCD calculations, Phys. Rev. D **98**, 074021 (2018).
[59] J. Liang, T. Draper, K.-F. Liu, A. Rothkopf, and Y.-B. Yang (XQCD Collaboration), Towards the nucleon hadronic tensor from lattice QCD, Phys. Rev. D **101**, 114503 (2020).
[60] T. Izubuchi, X. Ji, L. Jin, I. W. Stewart, and Y. Zhao, Factorization theorem relating Euclidean and light-cone parton distributions, Phys. Rev. D **98**, 056004 (2018).
[61] J. Karpie, K. Orginos, and S. Zafeiropoulos, Moments of Ioffe time parton distribution functions from non-local matrix elements, J. High Energy Phys. 11 (2018) 178.
[62] B. Joó, J. Karpie, K. Orginos, A. Radyushkin, D. Richards, and S. Zafeiropoulos, Parton distribution functions from Ioffe time pseudo-distributions, J. High Energy Phys. 12 (2019) 081.
[63] B. Joó, J. Karpie, K. Orginos, A. V. Radyushkin, D. G. Richards, R. S. Sufian, and S. Zafeiropoulos, Pion valence structure from Ioffe-time parton pseudodistribution functions, Phys. Rev. D **100**, 114512 (2019).
[64] B. Joó, J. Karpie, K. Orginos, A. V. Radyushkin, D. G. Richards, and S. Zafeiropoulos, Parton distribution functions from Ioffe time pseudodistributions from lattice calculations: Approaching the physical point, Phys. Rev. Lett. **125**, 232003 (2020).
[65] Z. Fan, X. Gao, R. Li, H.-W. Lin, N. Karthik, S. Mukherjee, P. Petreczky, S. Syritsyn, Y.-B. Yang, and R. Zhang, Isovector parton distribution functions of the proton on a superfine lattice, Phys. Rev. D **102**, 074504 (2020).
[66] C. Egerer *et al.* (HadStruc Collaboration), Transversity parton distribution function of the nucleon using the pseudodistribution approach, Phys. Rev. D **105**, 034507 (2022).
[67] X. Gao, A. D. Hanlon, N. Karthik, S. Mukherjee, P. Petreczky, P. Scior, S. Shi, S. Syritsyn, Y. Zhao, and K. Zhou, Continuum-extrapolated NNLO valence PDF of the pion at the physical point, Phys. Rev. D **106**, 114510 (2022).
[68] X. Gao, A. D. Hanlon, J. Holligan, N. Karthik, S. Mukherjee, P. Petreczky, S. Syritsyn, and Y. Zhao, Unpolarized proton PDF at NNLO from lattice QCD with physical quark masses, Phys. Rev. D **107**, 074509 (2023).
[69] H. Dutrieux, R. G. Edwards, C. Egerer, J. Karpie, C. Monahan, K. Orginos, A. Radyushkin, D. Richards, E. Romero, and S. Zafeiropoulos (HadStruc Collaboration), Towards unpolarized GPDs from pseudo-distributions, J. High Energy Phys. 08 (**2024**) 162.
[70] A. Shindler, Moments of parton distribution functions of any order from lattice QCD, Phys. Rev. D **110**, L051503 (2024).
[71] P. C. Barry *et al.* (Jefferson Lab Angular Momentum (JAM), HadStruc Collaborations), Complementarity of experimental and lattice QCD data on pion parton distributions, Phys. Rev. D **105**, 114051 (2022).
[72] R. Narayanan and H. Neuberger, Infinite N phase transitions in continuum Wilson loop operators, J. High Energy Phys. 03 (2006) 064.
[73] M. Lüscher, Properties and uses of the Wilson flow in lattice QCD, J. High Energy Phys. 08 (2010) 071; 03 (2014) 92.
[74] M. Lüscher and P. Weisz, Perturbative analysis of the gradient flow in non-Abelian gauge theories, J. High Energy Phys. 02 (2011) 051.

[75] M. Lüscher, Chiral symmetry and the Yang–Mills gradient flow, J. High Energy Phys. 04 (2013) 123.

[76] H. Suzuki, Energy–momentum tensor from the Yang–Mills gradient flow, Prog. Theor. Exp. Phys. **2013**, 083B03 (2013); **2015**, 079201(E) (2015).

[77] M. Lüscher, Future applications of the Yang-Mills gradient flow in lattice QCD, Proc. Sci. LATTICE2013 (**2014**) 016 [arXiv:1308.5598].

[78] In Ref. [70], the matching coefficients $\zeta_n$ are denoted by $c_n$.

[79] S. G. Gorishnii, S. A. Larin, and F. V. Tkachov, The algorithm for OPE coefficient functions in the MS scheme, Phys. Lett. B **124**, 217 (1983).

[80] S. G. Gorishnii and S. A. Larin, Coefficient functions of asymptotic operator expansions in minimal subtraction scheme, Nucl. Phys. **B283**, 452 (1987).

[81] R. V. Harlander, Y. Kluth, and F. Lange, The two-loop energy-momentum tensor within the gradient-flow formalism, Eur. Phys. J. C **78**, 944 (2018); **79**, 858(E) (2019).

[82] J. Artz, R. V. Harlander, F. Lange, T. Neumann, and M. Prausa, Results and techniques for higher order calculations within the gradient-flow formalism, J. High Energy Phys. 06 (2019) 121; 10 (2019) 32.

[83] E. G. Floratos, D. A. Ross, and C. T. Sachrajda, Higher order effects in asymptotically free gauge theories: The anomalous dimensions of Wilson operators, Nucl. Phys. **B129**, 66 (1977); **B139**, 545(E) (1978).

[84] A. Gonzalez-Arroyo, C. Lopez, and F. J. Yndurain, Second order contributions to the structure functions in deep inelastic scattering. I. Theoretical calculations, Nucl. Phys. **B153**, 161 (1979).

[85] H. Makino and H. Suzuki, Lattice energy-momentum tensor from the Yang-Mills gradient flow—inclusion of fermion fields, Prog. Theor. Exp. Phys. **2014**, 63B02 (2014); **2015**, 079202(E) (2015).

[86] J. Borgulat, R. V. Harlander, J. T. Kohnen, and F. Lange, Short-flow-time expansion of quark bilinears through next-to-next-to-leading order QCD, J. High Energy Phys. 05 (2024) 179.

[87] A. Francis, P. Fritzsch, R. Karur, J. Kim, G. Pederiva, D. A. Pefkou, A. Rago, A. Shindler, A. Walker-Loud, and S. Zafeiropoulos, companion paper, Moments of parton distributions functions of the pion from lattice QCD using gradient flow, Phys. Rev. D **113**, 074520 (2026).

[88] A. S. Francis, F. Cuteri, P. Fritzsch, G. Pederiva, A. Rago, A. Shindler, A. Walker-Loud, and S. Zafeiropoulos, Properties, ensembles and hadron spectra with stabilised Wilson fermions, Proc. Sci. LATTICE2021 (**2022**) 118 [arXiv:2201.03874].

[89] F. Cuteri, A. S. Francis, P. Fritzsch, G. Pederiva, A. Rago, A. Shindler, A. Walker-Loud, and S. Zafeiropoulos, Gauge generation and dissemination in OpenLat, Proc. Sci. LATTICE2022 (**2023**) 426 [arXiv:2212.07314].

[90] F. Cuteri, A. Francis, P. Fritzsch, G. Pederiva, A. Rago, A. Shindler, A. Walker-Loud, and S. Zafeiropoulos, Benchmark continuum limit results for spectroscopy with stabilized Wilson fermions, Proc. Sci. LATTICE2022 (**2023**) 074 [arXiv:2212.11048].

[91] A. Francis, F. Cuteri, P. Fritzsch, G. Pederiva, A. Rago, A. Shindler, A. Walker-Loud, and S. Zafeiropoulos, Progress in generating gauge ensembles with stabilized Wilson fermions, Proc. Sci. LATTICE2023 (**2024**) 048 [arXiv:2312.11298].

[92] Y. Aoki *et al.* (Flavour Lattice Averaging Group (FLAG) Collaboration), FLAG review 2024, Phys. Rev. D **113**, 014508 (2026).

[93] T. Blum *et al.* (RBC, UKQCD Collaborations), Domain wall QCD with physical quark masses, Phys. Rev. D **93**, 074505 (2016).

[94] G. S. Bali, S. Collins, P. Georg, D. Jenkins, P. Korcyl, A. Schäfer, E. E. Scholz, J. Simeth, W. Söldner, and S. Weishäupl (RQCD Collaboration), Scale setting and the light baryon spectrum in $N_f = 2 + 1$ QCD with Wilson fermions, J. High Energy Phys. 05 (2023) 035.

[95] M. Bruno, T. Korzec, and S. Schaefer, Setting the scale for the CLS $2 + 1$ flavor ensembles, Phys. Rev. D **95**, 074504 (2017).

[96] S. Borsányi, S. Dürr, Z. Fodor, C. Hoelbling, S. D. Katz, S. Krieg, T. Kurth, L. Lellouch, T. Lippert, and C. McNeile (BMW Collaboration), High-precision scale setting in lattice QCD, J. High Energy Phys. 09 (2012) 010.

[97] We set to $m = 2$, as we do not find any advantage in other choices.

[98] In the case of Ref. [14], the comparison employs the NLO + NLL double Mellin method.

[99] D. Brommel, M. Diehl, M. Göckeler, P. Hagler, R. Horsley, D. Pleiter, P. E. L. Rakow, A. Schäfer, G. Schierholz, and J. M. Zanotti, Structure of the pion from full lattice QCD, Proc. Sci. LAT2005 (**2006**) 360 [arXiv:hep-lat/0509133].

[100] D. Brommel, Pion structure from the lattice, Ph.D. thesis, Regensburg University, 2007.

[101] G. Bali, S. Collins, B. Glässle, M. Göckeler, N. Javadi-Motaghi, J. Najjar, W. Söldner, and A. Sternbeck, Pion structure from lattice QCD, Proc. Sci. LATTICE2013 (**2014**) 447 [arXiv:1311.7639].

[102] A. Abdel-Rehim *et al.*, Nucleon and pion structure with lattice QCD simulations at physical value of the pion mass, Phys. Rev. D **92**, 114513 (2015); **93**, 039904(E) (2016).

[103] M. Oehm, C. Alexandrou, M. Constantinou, K. Jansen, G. Koutsou, B. Kostrzewa, F. Steffens, C. Urbach, and S. Zafeiropoulos, $\langle x \rangle$ and $\langle x^2 \rangle$ of the pion PDF from lattice QCD with $N_f = 2 + 1 + 1$ dynamical quark flavors, Phys. Rev. D **99**, 014508 (2019).

[104] M. Löffler, P. Wein, T. Wurm, S. Weishäupl, D. Jenkins, R. Rödl, A. Schäfer, and L. Walter (RQCD Collaboration), Mellin moments of spin dependent and independent PDFs of the pion and rho meson, Phys. Rev. D **105**, 014505 (2022).

[105] C. Alexandrou, S. Bacchio, I. Cloet, M. Constantinou, K. Hadjiyiannakou, G. Koutsou, and C. Lauer (ETM Collaboration), Mellin moments $\langle x \rangle$ and $\langle x^2 \rangle$ for the pion and kaon from lattice QCD, Phys. Rev. D **103**, 014508 (2021).

[106] C. Alexandrou, S. Bacchio, I. Cloët, M. Constantinou, K. Hadjiyiannakou, G. Koutsou, and C. Lauer (ETM Collaboration), Pion and kaon $\langle x^3 \rangle$ from lattice QCD and PDF reconstruction from Mellin moments, Phys. Rev. D **104**, 054504 (2021).

[107] W. Detmold, W. Melnitchouk, and A. W. Thomas, Parton distribution functions in the pion from lattice QCD, Phys. Rev. D **68**, 034025 (2003).

[108] G. Martinelli, C. Pittori, C. T. Sachrajda, M. Testa, and A. Vladikas, A general method for nonperturbative renormalization of lattice operators, Nucl. Phys. **B445**, 81 (1995).

[109] G. Martinelli, S. Petrarca, C. T. Sachrajda, and A. Vladikas, Nonperturbative renormalization of two quark operators with an improved lattice fermion action, Phys. Lett. B **311**, 241 (1993); **317**, 660(E) (1993).
[110] H. Dutrieux, J. Karpie, K. Orginos, and S. Zafeiropoulos, Simple nonparametric reconstruction of parton distributions from limited Fourier information, Phys. Rev. D **111**, 034515 (2025).
[111] A. Candido, L. Del Debbio, T. Giani, and G. Petrillo, Bayesian inference with Gaussian processes for the determination of parton distribution functions, Eur. Phys. J. C **84**, 716 (2024).
[112] X.-D. Ji, Off forward parton distributions, J. Phys. G **24**, 1181 (1998).
[113] A. V. Radyushkin, Nonforward parton distributions, Phys. Rev. D **56**, 5524 (1997).
[114] A. Buckley, J. Ferrando, S. Lloyd, K. Nordström, B. Page, M. Rüfenacht, M. Schönherr, and G. Watt, LHAPDF6: Parton density access in the LHC precision era, Eur. Phys. J. C **75**, 132 (2015).
[115] www.gauss-centre.eu.
[116] Jülich Supercomputing Centre, JUWELS cluster and booster: Exascale pathfinder with modular supercomputing architecture at Juelich Supercomputing Centre, J. Large-Scale Res. Facil. **7**, A183 (2021).
[117] M. Lüscher, Code available at https://luscher.web.cern.ch/luscher/openQCD/.
[118] R. G. Edwards and B. Joó (SciDAC, LHPC, UKQCD Collaborations), The Chroma software system for lattice QCD, Nucl. Phys. B, Proc. Suppl. **140**, 832 (2005).
[119] M. Clark, R. Babich, K. Barros, R. Brower, and C. Rebbi, Solving lattice QCD systems of equations using mixed precision solvers on GPUs, Comput. Phys. Commun. **181**, 1517 (2010).
[120] R. Babich, M. Clark, B. Joó, G. Shi, R. Brower, and S. Gottlieb, Scaling lattice QCD beyond 100 GPUs, in *SC11 International Conference for High Performance Computing, Networking, Storage and Analysis* (2011), arXiv:1109.2935.
[121] M. A. Clark, B. Joó, A. Strelchenko, M. Cheng, A. Gambhir, and R. Brower, Accelerating lattice QCD multigrid on GPUs using fine-grained parallelization, arXiv:1612.07873.
[122] F. T. Winter, M. A. Clark, R. G. Edwards, and B. Joó, A Framework for Lattice QCD Calculations on GPUs, in *2014 IEEE 28th International Parallel and Distributed Processing Symposium, Phoenix, AZ, USA* (2014), pp. 1073–1082.
[123] A. Gambhir, D. Brantley, J. Chang, B. Hörz, H. Monge-Camacho, P. Vranas, and A. Walker-Loud, LALIBE, https://github.com/callat-qcd/lalibe (2018).
[124] C. R. Harris *et al.*, Array programming with NumPy, Nature (London) **585**, 357 (2020).
[125] P. Virtanen *et al.* (SciPy 1.0 Contributors), SciPy 1.0: Fundamental algorithms for scientific computing in Python, Nat. Methods **17**, 261 (2020).
[126] G. P. Lepage, GVAR v. 11.9.1, (2020), https://github.com/gplepage/gvar, 10.5281/zenodo.4290884.
[127] G. P. Lepage, LSQFIT v. 11.7, (2020), https://github.com/gplepage/lsqfit, 10.5281/zenodo.4037174.
[128] J. D. Hunter, Matplotlib: A 2D graphics environment, Comput. Sci. Eng. **9**, 90 (2007).
[129] G. Martinelli and C. T. Sachrajda, A lattice calculation of the pion's form-factor and structure function, Nucl. Phys. **B306**, 865 (1988).
[130] C. W. Bernard, T. Draper, G. Hockney, and A. Soni, Calculation of weak matrix elements: Some technical aspects, in *Workshop on Lattice Gauge Theories* (Springer US, Boston, MA, 1986).
[131] A. Francis, P. Fritzsch, R. Karur, J. Kim, G. Pederiva, D. A. Pefkou, A. Rago, A. Shindler, A. Walker-Loud, and S. Zafeiropoulos, Probing higher moments of pion parton distribution functions, Proc. Sci. LATTICE2024 (**2025**) 336 [arXiv:2412.01750].
[132] K. Symanzik, Continuum limit and improved action in lattice theories: I. Principles and $\varphi^4$ theory, Nucl. Phys. **B226**, 187 (1983).
[133] K. Symanzik, Continuum limit and improved action in lattice theories: II. O($N$) nonlinear sigma model in perturbation theory, Nucl. Phys. **B226**, 205 (1983).
[134] M. Luscher, S. Sint, R. Sommer, and P. Weisz, Chiral symmetry and O($a$) improvement in lattice QCD, Nucl. Phys. **B478**, 365 (1996).
[135] A. Francis, P. Fritzsch, M. Lüscher, and A. Rago, Master-field simulations of O($a$)-improved lattice QCD: Algorithms, stability and exactness, Comput. Phys. Commun. **255**, 107355 (2020).

## End Matter

*Appendix A: Lattice QCD technical details*—In this appendix, we provide additional details on the lattice calculation underlying the results presented in the main text.

The main building block in the calculation of the ratio of moments presented in this Letter is the correlation function

$$C_n^{uu}(t;x_4=\tau_s,y_4=\tau_{\mathcal{O}}) = a^6\sum_{\mathbf{x},\mathbf{y}} e^{i\mathbf{p}\cdot(\mathbf{x}-\mathbf{y})}\langle P^{du}(\mathbf{x},x_4)\hat{\mathcal{O}}_n^{uu}(t,\mathbf{y},y_4)P^{ud}(0)\rangle_c, \quad \text{(A1)}$$

where the subscript $c$ indicates that only the fermionic connected contribution is included.

In the nonsinglet case, there is no mixing with gluonic twist-2 operators, and the matrix elements for a spin-0 hadron are given by

$$\langle h(p)|\hat{O}_n^{uu}|h(p)\rangle = 2(p_{\mu_1}\cdots p_{\mu_n} - \text{traces})\langle x^{n-1}\rangle, \quad \text{(A2)}$$

with $h(p)$ being a hadronic state of momentum $p$, and $\hat{O}_n$ the trace-subtracted operator of Eq. (2).

In standard lattice QCD calculations, the renormalization and continuum limit of these operators is greatly

complicated. For $n > 2$, twist-2 operators mix with lower-dimensional operators, and this mixing is power-divergent in the lattice spacing $a$, preventing a controlled continuum limit. For $n = 3$, 4, specific irreducible representations (irreps) can be chosen to avoid such mixing [48,129]; however, only operators with all indices different transform irreducibly, which requires injecting spatial momentum in multiple directions in Eq. (A2). This leads to a severe deterioration of the signal-to-noise ratio, as confirmed in recent lattice studies [105,106]. For $n > 4$, no irreps are available that are safe from power-divergent mixing, and consequently the extraction of higher Mellin moments of PDFs with local operators has remained out of reach.

With the method adopted in this Letter, we are not constrained in the choice of Lorentz indices and can therefore select twist-2 operators with all temporal indices.

In the evaluation of the correlation function in Eq. (A1), we project to vanishing spatial momentum [Eq. (6)]. For the calculation of the quark propagators, we use a single randomly positioned, unsmeared $\mathbb{Z}_4$ stochastic noise source per configuration, although for notational simplicity in Eq. (6), the source is written as if it were fixed at the origin.

The three-point functions are measured at two sink-source separations per ensemble, using the sequential source-through-the-sink method [130], and at several flow times up to $t/t_0 \simeq 2.7$, spaced in steps of $\sim 0.1$.

Constructing the traceless operator bases for $n \in [2, 6]$ requires 4, 10, 40, 136, and 544 independent operators with unique Lorentz indices, which constitutes a major part of the computational cost. Moreover, each three-point function contains several terms arising from the discretized symmetrized covariant derivatives, with each term itself a sum of four contributions. To reduce this contraction cost, we employ several numerical improvements, detailed in Refs. [87,131].

If the flow-time footprint of $\hat{\mathcal{O}}_n^{uu}(t)$ is sufficiently smaller than its Euclidean time separation from the pion creation and annihilation operators—i.e., $\sqrt{8t} \ll \tau_s - \tau_{\mathcal{O}}$ and $\sqrt{8t} \ll \tau_{\mathcal{O}}$—the three-point function of Eq. (6) admits the spectral decomposition

$$C_n^{uu}(t;\tau_s,\tau_{\mathcal{O}}) = \sum_{k,k'} \frac{e^{-E_{k'}\tau_s} e^{-(E_k - E_{k'})\tau_{\mathcal{O}}}}{4E_k E_{k'}} \times Z_k^* Z_{k'} \langle k'(\mathbf{0})|\hat{\mathcal{O}}_n^{uu}(t)|k(\mathbf{0})\rangle, \quad \text{(A3)}$$

where $Z_k = \langle 0|P^{du}|k(\mathbf{0})\rangle$, and the sum runs over all states $k$ in the spectrum. The ground-state contribution can then be isolated in the limit $\tau_s \gg \tau_{\mathcal{O}} \gg 0$. In this regime, for each flow time $t/a^2$, the ratio of three-point functions becomes independent of $\tau_{\mathcal{O}}$ (and of $\tau_s$), leading to the ratio of matrix elements $A_n(t)/A_2(t)$ given in Eq. (7). Fits including excited states give results consistent with simple plateau fits, showing that, within the present statistical precision, the extracted matrix-element ratios are not significantly affected by excited-state effects. As discussed in the "Lattice QCD calculation" section of the main text, we adopt a conservative analysis strategy (see Ref. [87] for details), chosen to reduce sensitivity to residual statistical fluctuations in some plateaus, at the expense of slightly larger uncertainties.

*Appendix B: Continuum limit*—In this appendix, we summarize our continuum extrapolation strategy and the treatment of cutoff effects for the correlation function entering our analysis. We first outline the Symanzik effective theory expectations for the lattice artifacts relevant to our setup, then describe the specific simplifications that occur for ratios of flowed moments, and finally state the practical extrapolation procedure adopted in this Letter.

The cutoff effects of the correlation function in Eq. (6) can be analyzed within Symanzik effective theory [132–134]. For the exponential-clover (exp-cl) fermion

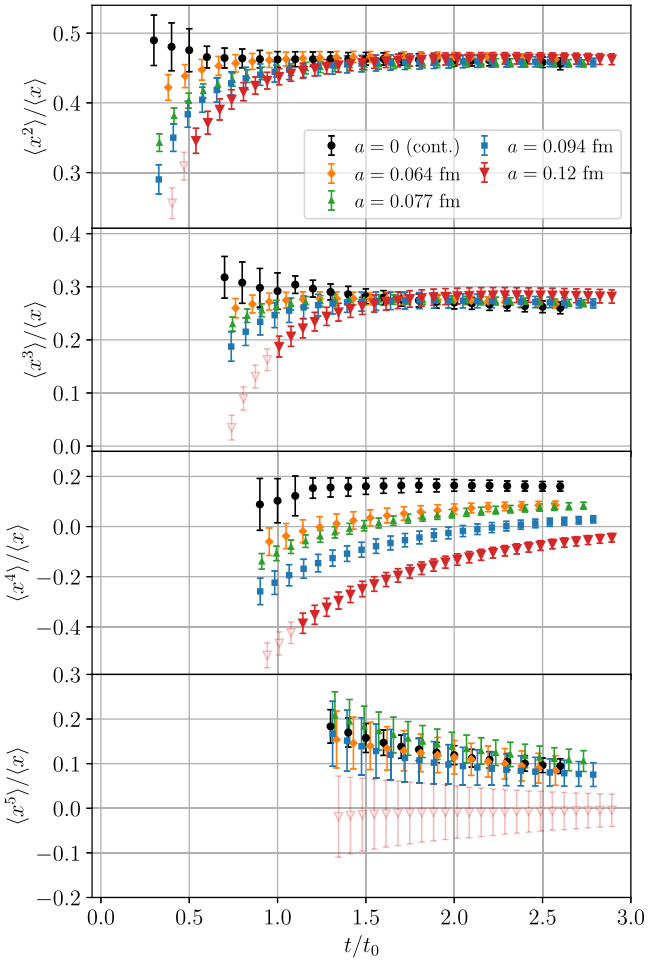



FIG. 4. Ratios of flowed Mellin moments $\langle x^{n-1}\rangle/\langle x\rangle$ for $n = 3$, 4, 5, 6 as functions of the flow time $t/t_0$. Results are shown for four lattice spacings, $a \simeq [0.064, 0.077, 0.094, 0.12]$ fm, and for their continuum extrapolation ($a = 0$). Points in lighter colors are excluded from the continuum limit (see main text).

action employed in this Letter [135], these effects can be discussed following the framework presented in Ref. [75]. Once the lattice action is nonperturbatively $O(a)$ improved, as is the case here with the exp-cl action, the remaining $O(a)$ cutoff effects related to flowed operators are of order $O(am)$. There are potentially short-distance $O(a)$ effects that decay faster than exponentially with the Euclidean separations between the operator and the source, $\tau_{\mathcal{O}}$, and between the operator and the sink, $\tau_s - \tau_{\mathcal{O}}$. We have checked numerically that the correlation function describing these effects is negligible in the range of $\tau_{\mathcal{O}}$ where we extract the matrix elements.

Besides further simplifying renormalization, the lattice calculation of ratios of flowed moments is also advantageous, because $O(am)$ discretization effects cancel, as they depend only on the fermion content of the flowed operators [75]. This implies cutoff effects that are parametrically of $O(a^2)$ [70]. This situation is particularly favorable compared to the standard case, where the calculation of matrix elements of twist-2 operators requires a nonperturbative subtraction of $O(a)$ cutoff effects that depend on the moment $n$ under consideration.

In Fig. 4, we show the flow-time dependence of the ratios of flowed moments, $r_n = \langle x^{n-1}\rangle/\langle x\rangle$, at each lattice spacing together with the resulting continuum limit (black points). The $O(a^2)$ discretization errors for these ratios can be parametrized as

$$r_n(a^2, t/t_0) = \frac{\langle x^{n-1}\rangle}{\langle x\rangle}(t/t_0) + \delta_2(t/t_0)\frac{a^2}{t_0} + \cdots, \quad \text{(B1)}$$

where $\delta_2(t/t_0)$ includes contributions that are power-enhanced—i.e., proportional to $a^2/t$. The observed flow-time dependence of $r_n$ in Fig. 4 confirms this expectation.

For the purpose of this Letter, we adopt a simple procedure in which each moment is extrapolated to the continuum limit independently at every flow time. The extrapolation uses the set of lattice spacings closest to the continuum that are well described by Eq. (B1), with a trend toward including more lattice spacings at larger flow times. The range in $t/t_0$ for which this approach is valid depends on both the moment and the flow time, and it defines the $(t/t_0)_{\text{min}}$ used in the subsequent extrapolation to vanishing flow time. The results presented here are consistent, in both central values and uncertainties, with the more detailed analysis presented in the companion paper [87], which provides a comprehensive assessment of the systematic uncertainties associated with the continuum extrapolation.